Fuel 368 (2024) 131672

Contents lists available at ScienceDirect

Fuel

journal homepage: www.elsevier.com/locate/fuel

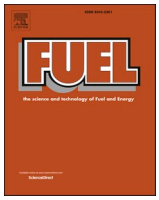

Full Length Article

Laminar flame speed regime at elevated temperature and pressure

Jacob Klein, Omid Samimi-Abianeh *

Department of Mechanical Engineering, Wayne State University, Detroit, MI 48202, USA

ARTICLE INFO

Keywords:
Laminar flame speed
Propane
n-heptane
Elevated temperature
Elevated pressure

ABSTRACT

Elevated temperature and pressure laminar flame speed measurements of propane and n-heptane fuel blends were conducted using a Rapid Compression Machine-Flame (RCM-Flame) apparatus. Herein, the lack of experimental flame speed data at simultaneously high temperatures and pressures akin to practical combustion conditions is addressed. The RCM-Flame apparatus is validated against a larger constant volume combustion chamber (CVCC) and simulations using a propane-nitrogen-oxygen mixture at ambient temperature and different pressures, demonstrating high fidelity. Further experiments with an n-heptane-nitrogen-helium-oxygen mixture reveal agreement between experimental and simulated flame speeds at semi-elevated, post-compression conditions. Trials with a propane-helium-oxygen mixture over varied temperatures and pressures demonstrate measured flame speeds falling between two kinetic mechanism simulations, maintaining the general trend. A power-law model correlating laminar flame speeds with elevated temperatures and pressures is developed for propane-helium-oxygen flames at a unity equivalence ratio. Overall, the kinetic mechanisms are shown to be able to predict flame speeds at elevated temperatures and pressures providing validation at conditions not yet explored in literature, optimistically advancing combustion research for practical applications.

1. Introduction

Laminar flame speed is a fundamental characteristic of the hydrocarbon combustion process and is therefore critical in combustion research and kinetic model development. Governed by chemical reactions, as well as thermodynamic, kinetic, and transport properties, it is described as the speed at which a planar flame front propagates through a fuel–air mixture under quiescent conditions. Flame speed measurements are reported in the literature using a variety of experimental devices such as Bunsen burners [1], diverging channels [2], constant volume combustion chambers [3], spherical bombs [4], and shock tubes [5], among others. Reported measurements cover an array of fuels such as propane, methane, n-heptane, hydrogen, etc., at primarily low-to-intermediate temperatures of 300–500 K, and pressures of 0.2–5 bar. [6] Overall, substantial work has been done on the topic and measurement of laminar flame speeds. However, at present there is a significant lack of experimental flame speed data at simultaneously high temperatures and pressures akin to practical combustion conditions. The majority of flame speed literature is focused on the effect of temperature or pressure independently, and the studies that investigate both are often at a fraction of the thermodynamic conditions seen in engines, turbines, and feasible applications. Moreover, the kinetic mechanisms currently available are generally validated in the low-to-intermediate temperature and pressure ranges described above which calls into question their dependability at elevated conditions. Thus, the central objective of this work is to obtain flame speed data at simultaneously elevated temperatures and pressures for comparison with computational modeling at the same conditions. In the following some of the relevant works are reviewed briefly.

Lowry et al. [7] investigated flame speeds of methane, ethane, and propane fuel blends at ambient gas temperature and ambient-to-elevated pressures of 1–10 atm. Using a constant volume cylindrical vessel with optical access, flame propagation was recorded using a Z-type Schlieren system. Unstretched flame speeds were calculated using linear regression of an integrated burning velocity versus stretch rate relation. The experimental results matched well with simulated flame speeds obtained with a reduced NUIG C_4 mechanism [8] as well as other published works. Furthermore, a flame speed model $S_u^0 = (a + b\varphi + c\varphi^2)(1/P_u)^{(d+e\varphi+f\varphi^2)}$ was developed describing the effects of equivalence ratio (φ) and unburned gas pressure (P_u) on flame speeds. The coefficients a, b, c, d, e, and f were curve fit parameters for each fuel blend. Peak flame speeds values were consistently observed for slightly rich mixture compositions at an equivalence ratio around 1.1 and flame speeds decreased with an increase in pressure.

* Corresponding author at: Department of Mechanical Engineering, Wayne State University, 5050 Anthony Wayne Drive, Detroit, MI 48202, USA.
E-mail addresses: jacob_klein@wayne.edu (J. Klein), O.Samimi@Wayne.edu (O. Samimi-Abianeh).

https://doi.org/10.1016/j.fuel.2024.131672
Received 18 January 2024; Received in revised form 5 April 2024; Accepted 7 April 2024
Available online 10 April 2024

Rather than examining the effect of pressure, as performed by Lowery et al. [7], Akram et al. [9] measured pure and diluted propane-air flame speeds over a range of gas temperatures (370–650 K) and equivalence ratios (0.7–1.3). A preheated mesoscale diverging channel facilitated their flame speed investigation. The studied conditions were simulated with a C_3 mechanism [10] and flame speeds were calculated based on a mass flux approach. Their results matched well with the computational and similar experimental results under a reported 5 % uncertainty. A model of the form $S_u^0/S_{u,r}^0 = \left(T_u/T_{u,r}\right)^\alpha$ was fit to the data where $S_{u,r}^0$ is the flame speed at a reference temperature $T_{u,r}$, and α is an empirical temperature exponent. With a reference temperature of 300 K, a temperature exponent of 1.636 maintained the trend of the measured results for stoichiometric propane-air. Additionally, flame speeds were again shown to be maximized for slightly rich mixtures across the studied temperature range.

To explain the effects of low-to-intermediate temperatures and pressures on flame speed simultaneously, Tang et al. [11] analyzed propane-hydrogen-air flames at equivalence ratios of 0.8 and 1.2, gas temperatures between 300 and 440 K, and pressures of 1 to 7.5 bar. Their experimental setup consisted of a cylindrical combustion vessel fitted with heating elements, a spark ignition system, and a pressure transducer. High-speed Schlieren imaging was utilized to record flame propagation. Flame speeds were obtained from linear fittings of measured burning velocity and stretch rate data. It was found that laminar flame speeds increased with the increase initial temperature and decreased with the increase of initial pressure over all the mixture compositions. Additionally, hydrodynamic instabilities were enhanced with the increase of initial pressure.

More recently, flame speed regimes at high temperature have started being studied. Ferris et al. [5] investigated methane and propane laminar flame speeds behind reflected shock waves in a shock tube at elevated unburned gas temperatures. Three mixture compositions: methane–nitrogen–oxygen at an equivalence ratio of one, propane-nitrogen–oxygen at an equivalence ratio of one, and propane-nitrogen-helium–oxygen at an equivalence ratio of 0.8, were considered at gas temperatures in the range of 391–832 K. The shock heated gas mixtures were spark ignited using a high-powered laser at ambient gas pressure. Flame propagation was recorded using high-speed chemiluminescence imaging. Laminar flame speeds were extrapolated from burning velocity versus stretch rate data and simulated at the studied conditions using NUIG's AramcoMech 3.0 [12] and LLNL's n-alkane [13] kinetic mechanisms. While steadily high relative to the models, the methane-air flame speed measurements displayed the same trend seen in the simulated results, with a maximum relative difference of 14.7 % from the AramcoMech 3.0 model. The propane results agreed well with the simulations and overlapped both with the reported uncertainties. Flame speeds were seen to increase with increases in gas temperature as expected. Additionally, the same power-law correlation used by Akram et al. [9] was fitted to the propane data. A temperature exponent value of $\alpha = 1.6$ effectively predicted the flame speed data with reference parameters taken at 300 K.

Recognizing the absence of measurements at simultaneously elevated temperatures and pressures in the above works, it is of interest to analyze the effects of practical thermodynamic conditions on flame speed regimes – further validating kinetic mechanisms at conditions not yet explored in the literature. In turn, the primary focus of this investigation is acquiring flame speed measurements at elevated temperatures and pressures with propane and n-heptane fuel blends using a Rapid Compression Machine-Flame (RCM-Flame) apparatus. Propane and n-heptane were chosen due to the magnitude of the publications studying these fuels and the comprehensive validation of kinetic mechanisms describing their flame speeds at low-to-intermediate thermodynamic conditions (e.g. [14–19]). There have been some concerns regarding the smaller geometry of the RCM-Flame and further suggestions that it may be ill-suited for flame speed measurements. Therefore, the RCM-Flame was initially validated against a larger constant volume combustion chamber (CCVC) as well as kinetic mechanisms using a propane-nitrogen–oxygen mixture. Upon demonstrating high fidelity of the flame speed data from the RCM-Flame, flame speeds at semi-elevated temperatures and pressures were measured and further compared to simulations with an n-heptane-nitrogen-helium–oxygen mixture. Lastly, a power-law correlation encompassing the effects of simultaneously elevated temperatures and pressures on propane-helium–oxygen laminar flames was developed. Numerical simulations were performed using two kinetic mechanisms when applicable: LLNL's detailed heptane kinetic mechanism [20] and NUIG's AramcoMech 3.0 mechanism [12]. A review of relevant literature and the purpose of this work were discussed above to familiarize the reader with an overview of laminar flame speed measurements and the merit(s) of this investigation. In subsequent sections of this paper the experimental facilities, the flame speed extraction methodology, the computational methodology, and the laminar flame speed results are detailed.

2. Experimental setup

A constant volume combustion chamber (CVCC) and a Rapid Compression Machine-Flame (RCM-Flame) apparatus were used to measure laminar flame speeds in this work. Three series of experiments were performed that fall into two categories: (1) laminar flame speed measurements at ambient temperature using the CVCC and RCM-Flame and (2) laminar flame speed measurements using the RCM-Flame at elevated gas temperatures and pressures. The mixtures for each series are reported in Table 1 along with the temperature and pressure ranges at the time of spark ignition. All mixtures had an equivalence ratio of one. The two devices (CVCC and RCM-Flame) are explained briefly in this section.

Flame speeds at ambient temperature and ambient-to-elevated pressures were measured in a constant volume combustion chamber (CVCC). The CVCC measures 7-inches and 5.5 in. in maximum and minimum dimensions, respectively. A more detailed description of the device can be found in [3]. Two 0.75-inch thick, 2.5-inch diameter, sapphire optical accesses allow viewing of combustion events inside the chamber. The chamber is outfitted with a spark ignition system and a dynamic pressure transducer. The experimental set up of the CVCC for this work is schematically shown in Fig. 1.

Flame speeds at ambient and elevated thermodynamic conditions were studied with the RCM-Flame. The device has been used previously to study laminar flame speeds over a range of conditions [21,22]. It operates by pneumatically driving and hydraulically stopping a piston to compress a gaseous mixture, simulating the compressive stroke of an internal combustion engine, while simultaneously spark igniting the mixture. The chamber of the device measures 2 in. in diameter and the piston's stroke length is 10 in. A 0.75-inch thick and 2-inch diameter sapphire optical window is fitted to the front of the device allowing view into the chamber and recording of flame propagation. Spark ignition of spherically expanding flames is facilitated by two opposing horizontally oriented electrodes separated by 1.5 mm. Additionally, the device is fitted with a dynamic pressure transducer, thermocouples measuring gas and wall temperatures, and heating bands. The RCM-Flame's piston can be locked, allowing the device to be used as a constant volume chamber.

Table 1
Test series mixture compositions and fixtures.

Series	Mixture composition [Partial Pressure, bar]	Instrument	P_u [bar]	T_u [K]
1	C_3H_8 (0.0806), O_2 (0.4030), N_2 (1.5164)	RCM-Flame, CVCC	1.0–1.5	300
2	n-C_7H_{16} (0.0319), O_2 (0.3504), He (1.0676), N_2 (0.2502)	RCM-Flame	5.0	633
3	C_3H_8 (0.0806), O_2 (0.4030), He (1.5164)	RCM-Flame	1.0–15.5	300–735

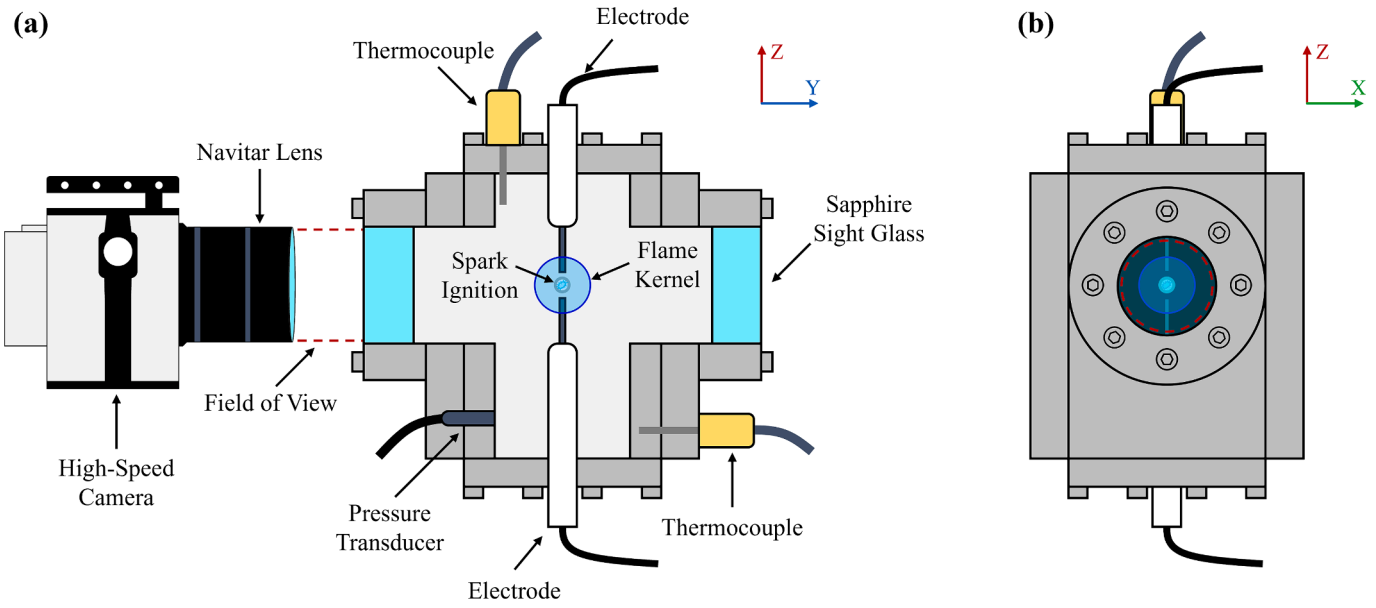

Fig. 1. Schematic of CVCC experimental set up: (a) side view, and (b) front view.

Further details of how the device operates can be found in [21]. Fig. 2 shows a schematic of the device. Additionally, the RCM-Flame's compression has been shown to be isentropic through computational fluid dynamics modeling. The creviced piston in the system reduces the formation of roll-up vortices during the compression stroke and ensures an adiabatic gas core.

A 5-gallon stainless steel vessel was used to prepare fuel mixtures based on partial pressures. Airgas supplied all gases (ultrahigh purity and research-grade) for mixtures, including nitrogen (research, 99.9997 %), oxygen (ultra-high purity, 99.994 %), helium (research, 99.9999 %), and propane (research, 99.99 %). n-Heptane used was of chemically pure grade (99.99 %), provided by Sigma-Aldrich, and injected into the mixing vessel in atomized form. An Agilent vacuum pump (DS 202) emptied the mixing vessel, as well as the CVCC and RCM-Flame prior to experiments. Omega K-type thermocouples (KMQSS-125G-6, uncertainty of ±1.1 °C) measured initial gas temperature in the CVCC and RCM-Flame. Chamber wall temperatures were recorded by low-accuracy Omega K-type thermocouples (uncertainty of ±2.2 °C). Static pressures for mixing and initial mixture introduction into the chambers were measured by a high accuracy static pressure transducer (Omega PX409-050A10V-EH, uncertainty of ±0.05 %). A Kistler piezoelectric pressure transducer (6045B) paired with a Kistler charge amplifier (5018) measured gas pressure during combustion events inside both fixtures. This dynamic pressure sensing system has an uncertainty of 0.56 %, accounting for uncertainty in measurements, linearity, and thermal shock. NI LabVIEW software recorded all pressure and temperature data during experimentation. Spark ignition of the test gases was initiated by way of discharging a variable voltage capacitor through an ignition coil (MSD Ballast 2). This resulted in a spark across the electrodes inside the CVCC and RCM-Flame during respective tests. A PE0630 solid-state relay by VB Controls and a DG646 Stanford Research Systems delay generator governed the timing of spark ignition. Flame propagation was recorded by a Phantom VEO 410L high-speed camera equipped with a 50 mm Navitar lens. Footage was exported to individual frames using PCC software by Vision Research.

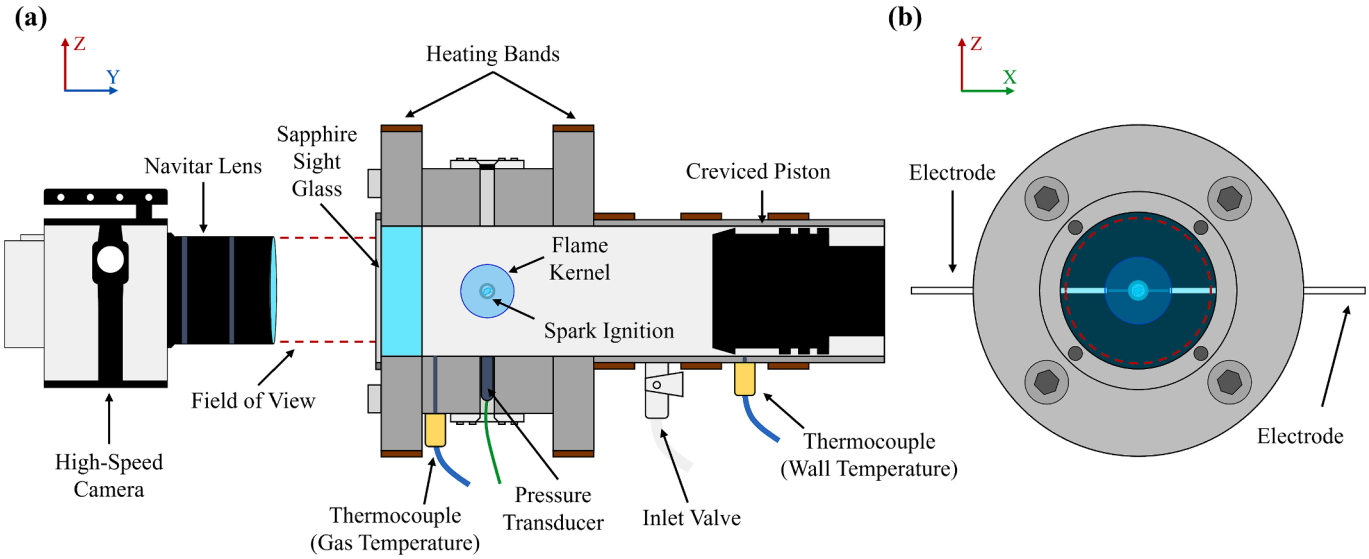

Fig. 2. Schematic of RCM-Flame experimental set up: (a) side view and (b) front view.

3. Measured data processing

The frames collected from the footage were processed using a developed code written in MATLAB [23] software. A series of sequential operations was performed on each frame to determine the flame location, size, and speed, as described in this section and shown in Fig. 3.

After frame sequences were imported into MATLAB [23], each frame was smoothed to reduce luminescent noise around the flame front. This was accomplished by convolving the image (8-bit unsigned integer matrix) with a 2-D Gaussian pixel kernel (standard deviation of $\sigma = 2$). The grayscale layer of the smoothed frame was extracted, and a global threshold was computed from a histogram of shades. This threshold was used to binarize the image into a live pixel region (i.e., where the flame is) and the background. The live region could then be outlined, and its centroid determined. Bounding this outline with a rectangle, the horizontal and vertical radii of the flame region were computed in pixels. The radius of the flame at every time step was taken to be the arithmetic mean of the bounding rectangle's half-lengths to account for any spherical asymmetries. The flame radius from each frame was then converted to physical units using a pixel/meter conversion factor (calculated based on the pixel diameters of the RCM-Flame or CCVC bores in each recording). Once the flame radius was extracted at each time step, the flame radius traces were smoothed using a second order Savitzky-Golay filter with a frame length of five. Lastly, the time rate of change of the flame's radius (burning velocity) was computed using second order finite difference formulas for numerical differentiation.

Two principal challenges arise in experimentally determining the flame speed of a spark ignited spherically expanding flame in a confined volume: (1) the effect of energy released from the spark ignition, and (2) the effect of the chamber size. Around the temporal location of the spark, flame propagation is turbulent and driven by the spark's rapid energy release. Then, as the flame propagates outward and nears the wall of the combustion chamber, pressure effects are considered which affect the expansion of the flame kernel. Thus, a data processing interval was instituted to isolate usable data for extrapolating laminar burning velocity (S_b^0) from the high-speed footage. The lower limit of data processing, denoted as τ_L, was determined based off the plot of the flame's radius versus the flame's stretch rate shown in Fig. 4 (a).

It has been suggested that a spherically expanding laminar flame maintains a constant burning velocity (S_b). [24] Under this assumption, if the parametrized functions $r(t)$ (flame radius) and $K(t) = 2S_b/r(t)$ (stretch rate) are plotted in a 2D plane, the resulting curve maintains a shape similar to a function of the form $f(x) = c/x$ where c is an arbitrary constant. However, experiments indicate that a spherically expanding laminar flame does not exhibit a constant burning velocity. [24] A change in the burning velocity as the radius increases would result in a change of slope of the above theorized function $f(x)$ as $K \longrightarrow 0$.

Fig. 4 (a) illustrates the effects of the spark energy release and chamber size on the flame radius versus stretch rate data in practice. The intermediate region of flame propagation features a shape that is similar to the theorized function $f(x)$ with the caveat that the slope changes as $K \longrightarrow 0$ (a consequence of the non-constant burning velocity). The start of this region defines τ_L and it greatly contrast the initial portion of the data

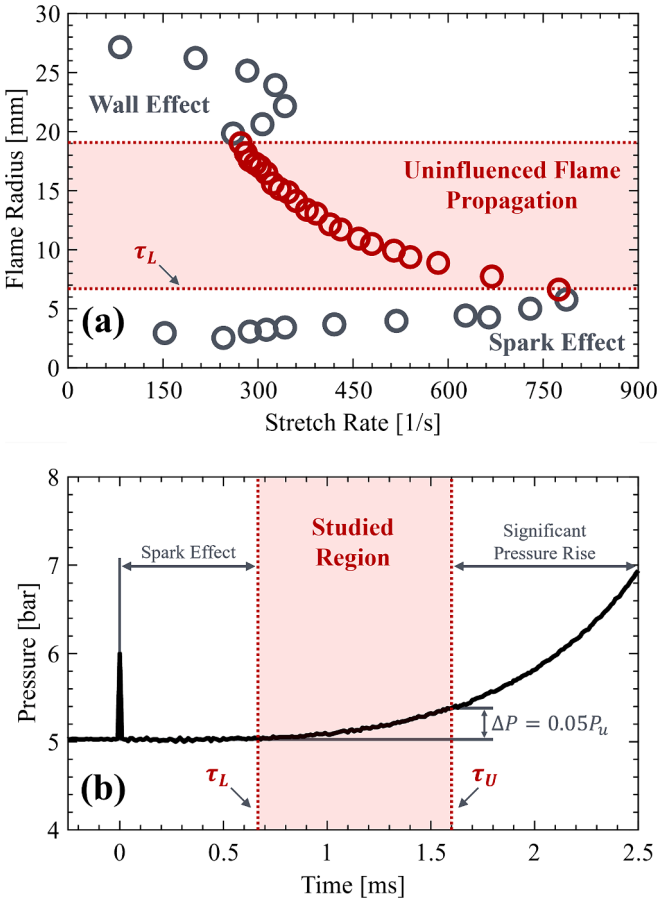

Fig. 4. Determination of data processing limits for an n-heptane-nitrogen-helium-oxygen flame at gas pressure and temperature of 5 bar and 636 K, respectively, using: (a) flame radius vs. stretch rate, and (b) pressure history.

when the spark drives the flame outwards resulting in an increase in radius and drastic increase in stretch rate. The upper limit, τ_U, is determined based on the pressure trace of the mixture and defined as the time when the mixture reached a pressure increase of roughly 5 % from the time of spark ignition, maintaining the quasi-isobaric condition. [21] Fig. 4 (b) graphically displays the region of interest in the data using the pressure trace.

Once the lower and upper post-processing regions were determined for each dataset, Markstein's model [24] was used,

$$S_b = S_b^0 - L_b\kappa \tag{1}$$

where L_b is the Markstein length and $\kappa = 1/r$ is the curvature, and Karlovitz's model [25] was used,

$$S_b = S_b^0 - L_K K \tag{2}$$

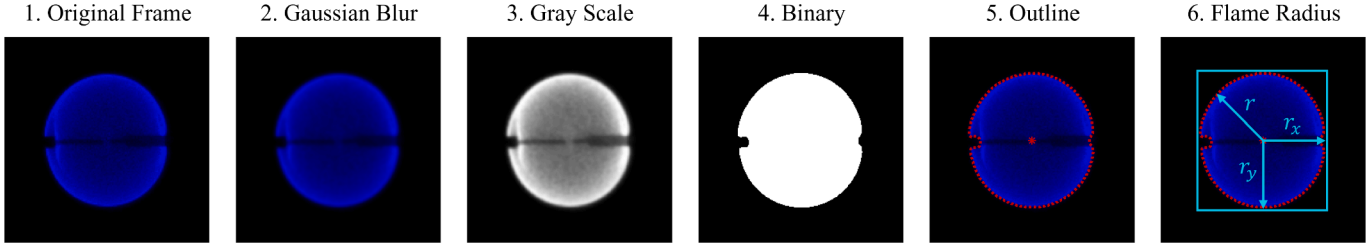

Fig. 3. Image processing operations to extract flame location, size, and speed for a propane-nitrogen-oxygen flame at unburned gas pressure (P_u) of 1.3 bar and unburned gas temperature (T_u) of 300 K.

where L_K is a constant to which the stretch response is attributed and $K = (2/r)(dr/dt)$ is stretch rate, to extrapolate laminar burning velocity (S_b^0) from a regression analysis of the burning velocity (S_b) versus curvature or stretch rate as shown in Fig. 5.

Unburned laminar flame speed S_u^0 was then calculated from S_b^0 through mass continuity,

$$\rho_u S_u^0 = \rho_b S_b^0 \tag{3}$$

where ρ_u and ρ_b are the unburned and burned gas densities, respectively. For the sake of spatial concerns, Markstein's model will be denoted as linear method one (LM1). Similarly, Karlovitz's model will be labeled linear method two (LM2).

4. Computational setup

Simulated flame speeds were obtained through 1-D propagating flame speed modeling in CHEMKIN-PRO [26] software. The model was supplied with the gas composition, temperature, and pressure at the time of spark ignition for each test. The simulation domain was initiated as an adiabatic tube of length 100 mm with uniform inlet conditions and at minimum 300 points. In locations where steady-state solutions diverged, grid points were increased to a maximum of 3000 mesh points progressively via automatic adaptive mesh refinement. Mixture-average transport properties were computed using the Curtiss-Hirschfelder method as described in [27]. Inclusion of the Soret effect proved to be negligible on simulated results, and thus was not simulated to reduce computational expense. For experiments involving the CVCC or the RCM-Flame with a locked piston (series 1), obtaining the simulated laminar flame speed was somewhat trivial as the same model could be used with simply the ambient temperature and spark-time pressure changed. However, to simulate the flame speeds at RCM-Flame conditions, an additional model was required. Homogenous batch reactor modeling, also performed in CHEMKIN-PRO [26], was utilized to simulate gas temperature and mixture composition post-compression to acquire the gas density and temperature at the time of spark ignition. As discussed, the RCM-Flame's compression is isentropic. Accordingly, the temperature and pressure are related by,

$$\ln\left(\frac{P_u}{P_i}\right) = \int_{T_i}^{T_u} \frac{\gamma(T)}{\gamma(T)-1}\frac{dT}{T} \tag{4}$$

where $\gamma(T)$ is the specific heat ratio of the gas at temperature T and the subscripts $(\bullet)_i$ and $(\bullet)_u$ denote pre-compression and spark-time properties, respectively. With the measured pressure profile, the mixture's temperature and density post-compression could be quantified, specifically at the time of spark ignition. To model the gas mixtures and flame speeds, LLNL's detailed heptane kinetic mechanism [20] was used for all three mixtures. NUIG's AramcoMech 3.0 mechanism [12] was also used for the propane mixtures.

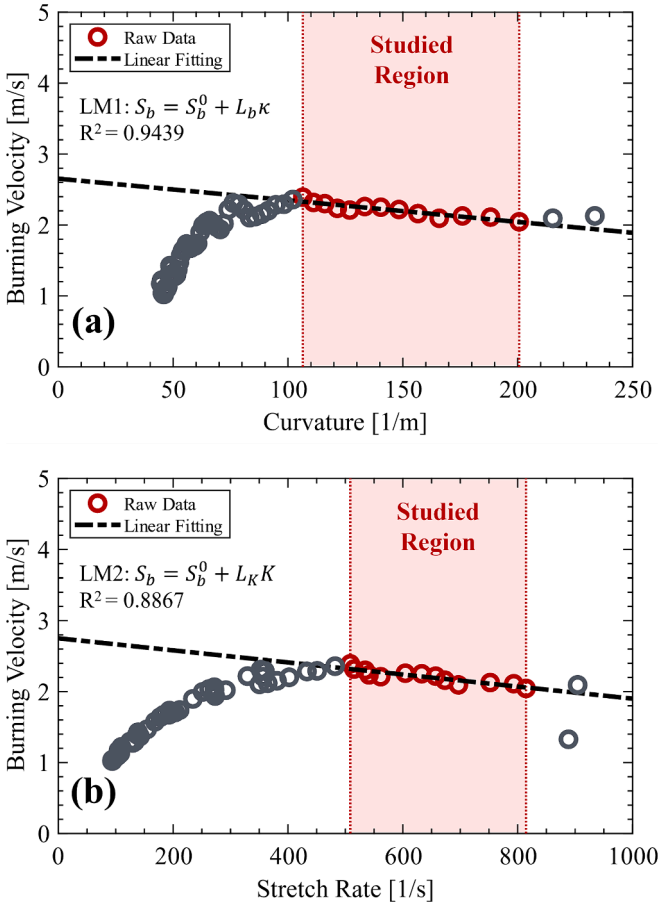

Fig. 5. Flame speed extrapolation using: (a) curvature, and (b) stretch rate for a propane-nitrogen- oxygen flame at gas pressure of 1.3 bar and temperature of 300 K.

5. Results and discussions

Laminar flame speed measurements were performed using three mixture compositions at a wide array of thermodynamic conditions and two experimental apparatuses. The experimental data, obtained by the previously outlined image processing and regression methodology, is presented, discussed, and compared to corresponding numerical data below.

Using a propane-nitrogen–oxygen mixture (as detailed previously in Table 1), the first set of experiments were performed to validate the RCM-Flame apparatus against simulation as well as a larger combustion chamber (CVCC). The mixture was at ambient temperature (300 K) and spark ignited at pressures of 1.0, 1.3, and 1.5 bar. The pressure profiles from the CVCC and RCM-Flame are compared in Fig. 6 (a). The traces from both fixtures agree well during the data collection interval as highlighted in the enlarged portion of the graph. The mixture's pressure rise in the RCM-Flame is initially more rapid than the CVCC, however reaches a fully burned state after the CVCC at the same condition. The corresponding flame speed data is shown in Fig. 6 (b). Error bars have been excluded from the plot to maintain clarity, but the maximum uncertainty of the measurements is 11.56 % (based on Coleman and Steele's uncertainty approach [28]).

The simulated flame speeds using the two mechanisms differed on average by 6.64 %. The measured data using both methods and both devices maintain the trend seen in simulation (decrease in flame speed as pressure increased). Overall, it is evident that flame speed data obtained using the RCM-Flame fixture matches the CVCC and simulation, which is indicative of high fidelity. The raw flame speed data is reported in Table 2.

To validate the RCM-Flame's measurement of flame speeds at elevated gas temperatures and pressures, empirical data of an n-heptane-nitrogen-helium–oxygen mixture's flame speed was compared to simulation. The pressure traces for these tests are shown in Fig. 7 (a). The black line represents an autoignition pressure trace (when there is no spark ignition), and the red lines (with different intensities) are the pressure histories of the flames. The results of the flame speed experiments and simulations are shown in Fig. 7 (b). Flames were studied at three ignition times, corresponding to three Damköhler numbers of 0.2476, 0.3933, and 0.6094. The Damköhler number is defined as the time of spark ignition normalized to the ignition delay (i.e., t_s/t_{ig}).

The measured and simulated flame speeds are in agreement within the uncertainty of the measurements (13.78 % maximum) at the studied conditions and differ by an average 11.07 %. Moreover, the data suggest

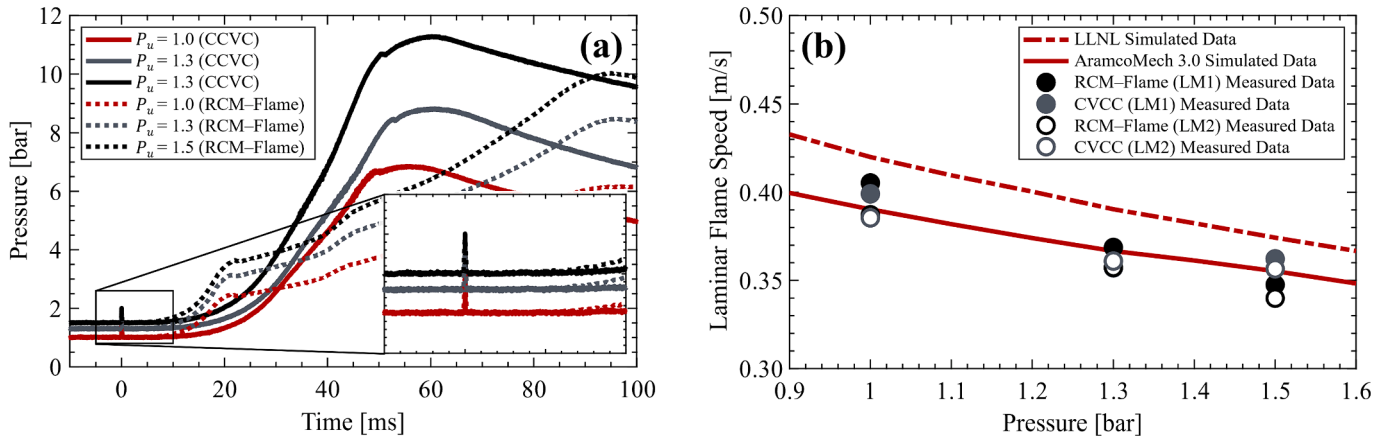

Fig. 6. (a) RCM-Flame and CVCC pressure histories at gas temperature of 300 K and gas pressures (P_u) of 1.0, 1.3, 1.5 bar, and (b) Comparison of simulated and measured laminar flame speeds using RCM-Flame and CVCC.

Table 2
Propane-nitrogen-oxygen averaged flame speed data of three experiments. Units of bar, kelvin, and m/s for pressure, temperature, and flame speed, respectively.

P_u	T_u	S_u^0(LLNL)	S_u^0(AramcoMech 3.0)	S_u^0(RCM-Flame LM1, LM2)	S_u^0(CVCC LM1, LM2)
1.0	300	0.4199	0.3903	0.4053, 0.3872	0.3991, 0.3855
1.3	300	0.3903	0.3666	0.3687, 0.3574	0.3571, 0.3610
1.5	300	0.3742	0.3552	0.3476, 0.3399	0.3622, 0.3566

that the flame speed remains quasi-constant prior to the first stage heat release (or Damköhler numbers less than ~0.7), as the temperature and pressure do not exhibit significant variability. The raw data for the experiments is reported in Table 3.

To further study flame speeds at elevated temperatures and pressures, experiments were conducted over a range of temperatures and pressures using a propane-helium–oxygen mixture. The pressure traces for this mixture are depicted in Fig. 8 (a). Spark ignition was initiated at 6 ms after the end of compression of the gas mixture in the RCM-Flame apparatus. The lower Damköhler of these flames removed the influence of autoignition on the data. The measured flame speeds at these spark pressures and temperature are compared to simulated values using LLNL and AramcoMech 3.0 in Fig. 8 (b).

The measured values fall in between the two kinetic mechanisms with a maximum uncertainty of 12.36 %. The general trend present in the simulated values over the varying pressures and temperature is maintained in the measured data. As LM1 uses flame curvature (strictly dependent on flame radius), the LM1 datasets feature less fluctuations than the LM2 datasets. LM2 introduces noise and truncation error from the numerical differentiation in stretch rate computations. The data is also presented in a two-dimensional format with Fig. 8 (c) & (d) for easier interpretation.

In the literature [6], laminar flame speeds are correlated to temperatures and pressures using the power-law model,

$$\frac{S_u^0}{S_{u,r}^0} = \left(\frac{T_u}{T_{u,r}}\right)^{\alpha} \left(\frac{P_u}{P_{u,r}}\right)^{\beta} \tag{5}$$

where the subscript $(\bullet)_{u,r}$ denotes reference conditions, and α as well as β are curve fit parameters. For this work, $T_{u,r} = 300$ K, $P_{u,r} = 1$ bar, and $S_{u,r}^0$ was measured at 1.2498 m/s using LM1. From the above, a model

Table 3
n-Heptane-nitrogen-helium-oxygen averaged flame speed data of three experiments.

P_u[bar]	T_u[K]	S_u^0(LLNL) [m/s]	S_u^0(LM1) [m/s]	S_u^0(LM2) [m/s]
5.0460	635.8	2.7140	2.4146	2.2818
5.0333	633.8	2.7030	2.4135	2.2432
4.9544	632.3	2.6951	3.3857	2.2088

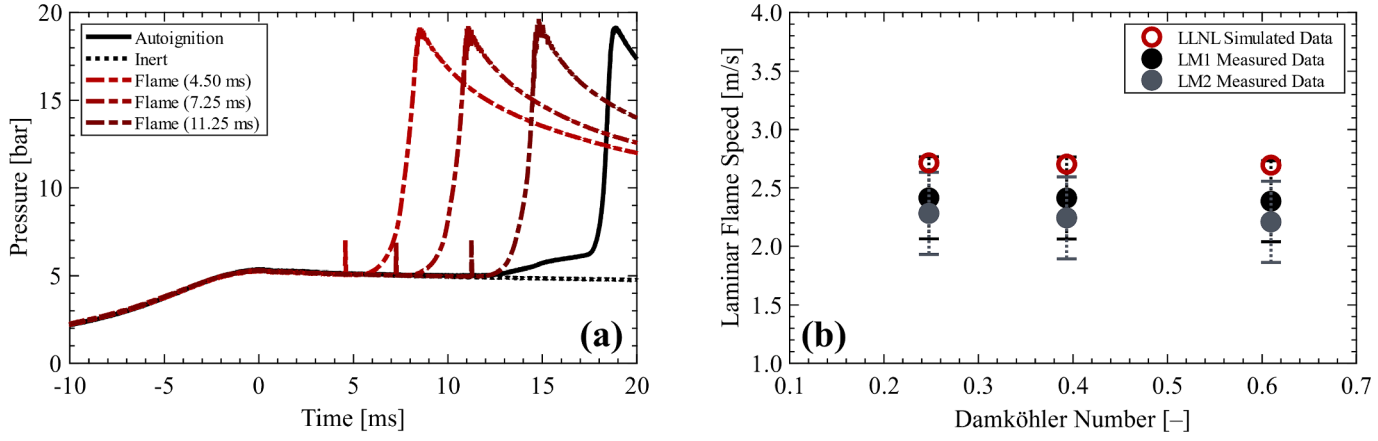

Fig. 7. (a) Pressure histories of n-heptane-nitrogen-helium-oxygen flames and autoignition at compressed gas pressure of 5.35 bar and compressed gas temperature of 643.8 K, and (b) measured and simulated laminar flame speeds.

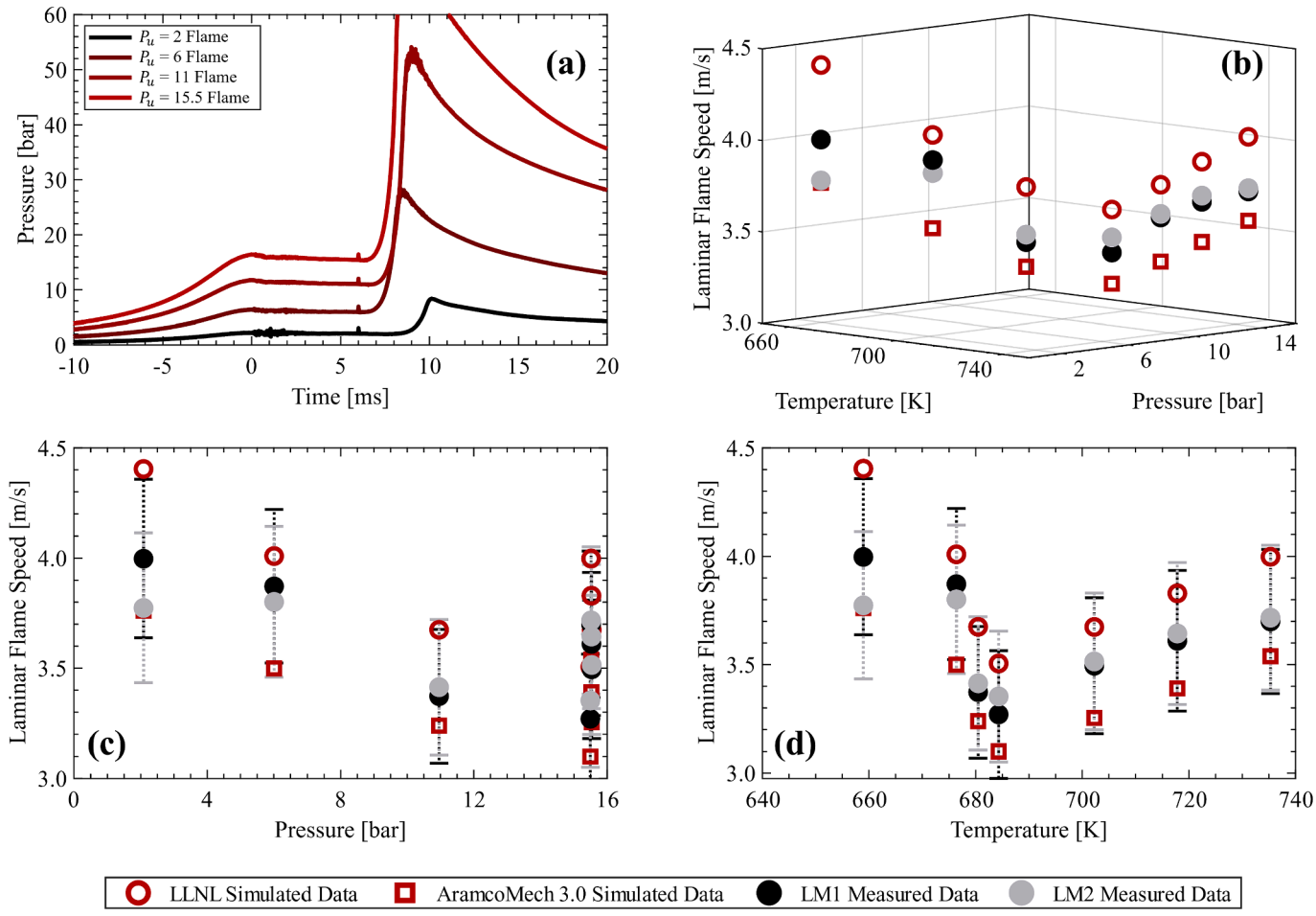

Fig. 8. (a) Flame pressure histories for propane-helium-oxygen, (b) measured and simulated flame speeds in 3d, (c) flame speed data vs. pressure, and (d) flame speed data vs. temperature.

was developed using the LM1 dataset in which $\alpha = 1.6206$ and $\beta = -0.1307$. A surface plot of Equation (5) for the propane-helium–oxygen dataset is presented in Fig. 9.

The experimental data is also reported in Table 4. It is noted that fitting the model to the LLNL data set resulted in parameters $\alpha = 1.5190$ and $\beta = -0.1380$. Similarly, the AramcoMech 3.0 simulated data produced values of $\alpha = 1.5145$ and $\beta = -0.1203$. The minimal difference between these values and those obtained experimentally, as well as the α values used by Ferris et al. [5] and Akram et al. [9], is indicative of overall agreement in the behavior of propane-helium–oxygen flames at equivalence ratios near unity.

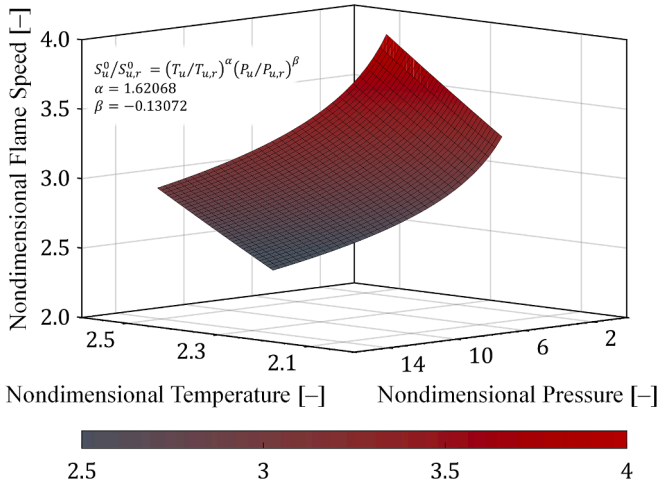

Fig. 9. Surface plot of laminar flame speed correlation at elevated temperatures and pressures for propane-helium-oxygen.

Table 4
Propane-helium-oxygen averaged flame speed data of three experiments.

P_u [bar]	T_u [K]	S_u^0(LLNL) [m/s]	S_u^0(AramcoMech 3.0) [m/s]	S_u^0(LM1) [m/s]	S_u^0(LM2) [m/s]
0.9989	300.0	1.4807	1.2539	1.2498	1.2267
2.0589	658.9	4.4039	3.7607	3.9975	3.7737
5.9932	676.3	4.0096	3.4992	3.8718	3.8010
11.0027	680.4	3.6746	3.2384	3.3725	3.4136
15.4408	684.3	3.5053	3.0995	3.2697	3.3527
15.4912	702.2	3.6738	3.2534	3.4947	3.5145
15.4906	717.7	3.8294	3.3902	3.6099	3.6436
15.5123	735.2	3.9984	3.5389	3.6993	3.7169

6. Summary

The laminar flame speed stands as a fundamental characteristic of the hydrocarbon combustion process. The parameter is undoubtedly significant in combustion research as well as kinetic mechanism development and validation. The aim of the current work was to acquire flame speed data under realistic combustion conditions using an RCM-Flame apparatus. The literature was surveyed to understand the various methods and means by which researchers measure flame speeds. Upon highlighting the existing lack of experimental data at

simultaneously elevated temperatures and pressures, the developed flame speed measurement methodology using the RCM-Flame and CVCC facilities was used to validate the RCM-Flame with a propane-nitrogen–oxygen mixture at ambient temperature and lower pressures. The results demonstrated excellent agreement between experimental data from both fixtures and numerical simulations. The RCM-Flame then demonstrated successful facilitation of flame speed measurements at semi-elevated gas temperatures and pressures for an n-heptane-nitrogen-helium–oxygen mixture. Further experiments were conducted with a propane-helium–oxygen mixture over a range of elevated temperatures and pressures. The measured flame speeds agreed with simulated values using LLNL's detailed heptane kinetic mechanism [20] and NUIG's AramcoMech 3.0 mechanism [12] kinetic mechanisms, falling between the two simulations with the general trend maintained. The developed temperature and pressure power-law correlation describes the measured and simulated values well, which, in addition to the partial conclusions from literature, indicates a comprehensive understanding of propane-helium–oxygen flame speed behavior at equivalence ratios near unity and elevated conditions. This work will hopefully contribute to the ongoing pursuit of further understanding the fundamentals of combustion processes across various thermodynamic conditions.

CRediT authorship contribution statement

Jacob Klein: Writing – original draft, Validation, Formal analysis, Data curation. **Omid Samimi-Abianeh:** Writing – review & editing, Supervision, Project administration, Funding acquisition, Conceptualization.

Declaration of competing interest

The authors declare that they have no known competing financial interests or personal relationships that could have appeared to influence the work reported in this paper.

Data availability

Data will be made available on request.

Acknowledgment

This material is based upon work supported by the United States National Science Foundation under Grant No. 2324471.

References

[1] Hu S, Gao J, Gong C, Zhou Y, Bai XS, Li ZS, et al. Assessment of uncertainties of laminar flame speed of premixed flames as determined using a Bunsen burner at varying pressures. Appl. Energy 2018;227:149–58. https://doi.org/10.1016/j.apenergy.2017.09.083.
[2] Akram M, Kumar S. Experimental studies on dynamics of methane–air premixed flame in meso-scale diverging channels. Combust. Flame 2011;158:915–24. https://doi.org/10.1016/j.combustflame.2011.02.011.
[3] Farhat A, Kumar REV, Samimi-Abianeh O. Laminar burning velocity measurement using the filtered broadband natural emissions of species. Energy Fuel 2020;34:3772–9. https://doi.org/10.1021/acs.energyfuels.9b04291.
[4] Lamoureux N, Djebaili-Chaumeix N, Paillard C-E. Laminar flame velocity determination for H2–air–He–CO2 mixtures using the spherical bomb method. Exp. Therm. Fluid Sci. 2003;27:385–93. https://doi.org/10.1016/S0894-1777(02)00243-1.
[5] Ferris AM, Susa AJ, Davidson DF, Hanson RK. High-temperature laminar flame speed measurements in a shock tube. Combust. Flame 2019;205:241–52. https://doi.org/10.1016/j.combustflame.2019.04.007.
[6] Konnov AA, Mohammad A, Kishore VR, Il KN, Prathap C, Kumar S. A comprehensive review of measurements and data analysis of laminar burning velocities for various fuel+air mixtures. Prog. Energy Combust. Sci. 2018;68:197–267. https://doi.org/10.1016/j.pecs.2018.05.003.
[7] Lowry W, de Vries J, Krejci M, Petersen E, Serinyel Z, Metcalfe W, et al. Laminar flame speed measurements and modeling of pure alkanes and alkane blends at elevated pressures. J. Eng. Gas Turbines Power 2011;133. https://doi.org/10.1115/1.4002809.
[8] Healy D, Donato NS, Aul CJ, Petersen EL, Zinner CM, Bourque G, et al. Isobutane ignition delay time measurements at high pressure and detailed chemical kinetic simulations. Combust. Flame 2010;157:1540–51. https://doi.org/10.1016/j.combustflame.2010.01.011.
[9] Akram M, Kishore VR, Kumar S. Laminar burning velocity of propane/CO_2/N_2–air mixtures at elevated temperatures. Energy Fuel 2012;26:5509–18. https://doi.org/10.1021/ef301000k.
[10] Qin Z, Lissianski VV, Yang H, Gardiner WC, Davis SG, Wang H. Combustion chemistry of propane: a case study of detailed reaction mechanism optimization. Proc. Combust. Inst. 2000;28:1663–9. https://doi.org/10.1016/S0082-0784(00)80565-2.
[11] Tang C, He J, Huang Z, Jin C, Wang J, Wang X, et al. Measurements of laminar burning velocities and Markstein lengths of propane–hydrogen–air mixtures at elevated pressures and temperatures. Int. J. Hydrogen Energy 2008;33:7274–85. https://doi.org/10.1016/j.ijhydene.2008.08.053.
[12] Zhou C-W, Li Y, Burke U, Banyon C, Somers KP, Ding S, et al. An experimental and chemical kinetic modeling study of 1,3-butadiene combustion: ignition delay time and laminar flame speed measurements. Combust. Flame 2018;197:423–38. https://doi.org/10.1016/j.combustflame.2018.08.006.
[13] Sarathy SM, Westbrook CK, Mehl M, Pitz WJ, Togbe C, Dagaut P, et al. Comprehensive chemical kinetic modeling of the oxidation of 2-methylalkanes from C7 to C20. Combust. Flame 2011;158:2338–57. https://doi.org/10.1016/j.combustflame.2011.05.007.
[14] Botha JP, Spalding DB, Egerton AC. The laminar flame speed of propane/air mixtures with heat extraction from the flame. Proc. R. Soc. Lond. A 1954;225:71–96. https://doi.org/10.1098/rspa.1954.0188.
[15] Amirante R, Distaso E, Tamburrano P, Reitz RD. Laminar flame speed correlations for methane, ethane, propane and their mixtures, and natural gas and gasoline for spark-ignition engine simulations. Int. J. Engine Res. 2017;18:951–70. https://doi.org/10.1177/1468087417720018.
[16] Zhao Z, Kazakov A, Li J, Fl D. The initial temperature and N2 dilution effect on the laminar flame speed of propane/air. Combust. Sci. Technol. 2004;176:1705–23. https://doi.org/10.1080/00102200490487553.
[17] Davis SG, Law CK. Laminar flame speeds and oxidation kinetics of iso-octane-air and n-heptane-air flames. Symp. (Int.) Combust. 1998;27:521–7. https://doi.org/10.1016/S0082-0784(98)80442-6.
[18] Kumar K, Freeh JE, Sung CJ, Huang Y. Laminar flame speeds of preheated iso-Octane/O2/N2 and n-Heptane/O2/N2 mixtures. J. Propul. Power 2007;23:428–36. https://doi.org/10.2514/1.24391.
[19] Smallbone AJ, Liu W, Law CK, You XQ, Wang H. Experimental and modeling study of laminar flame speed and non-premixed counterflow ignition of n-heptane. Proc. Combust. Inst. 2009;32:1245–52. https://doi.org/10.1016/j.proci.2008.06.213.
[20] Mehl M, Pitz WJ, Westbrook CK, Curran HJ. Kinetic modeling of gasoline surrogate components and mixtures under engine conditions. Proc. Combust. Inst. 2011;33:193–200. https://doi.org/10.1016/j.proci.2010.05.027.
[21] Goyal T, Samimi-Abianeh O. Methane laminar flame speed measurement at high gas temperature using rapid compression machine-flame (RCM-flame). Ind. Eng. Chem. Res. 2022;61:9981–90. https://doi.org/10.1021/acs.iecr.2c01117.
[22] T. Goyal, J. Klein, O. Samimi Abianeh, Numerical and Experimental study of autoignition-assisted premixed n-heptane flames using RCM-Flame apparatus, 13th US National Combustion Meeting, 2023.
[23] The MathWorks Inc. MATLAB 2023.
[24] Markstein GH. Non-steady flame propagation. Oxford: Pergamon Press; 1964.
[25] Karlovitz B, Denniston DW, Knapschaefer DH, Wells FE. Studies on turbulent flames. Symp. (Int.) Combust. 1953;4:613–20. https://doi.org/10.1016/S0082-0784(53)80082-2.
[26] CHEMKIN-PRO, Reaction Design, 2021.
[27] Hirschfelder JO, Curtiss CF, Bird RB. Molecular theory of gases and liquids. Phys. Today 1955;8:17. https://doi.org/10.1063/1.3061949.
[28] Coleman HW, Steele WG. Engineering application of experimental uncertainty analysis. AIAA J. 1995;33:1888–96. https://doi.org/10.2514/3.12742.